Ottawa, Canada
ACTIVE 2009
2009 August 20-22

Downscaling of decentralised feedback control units for active vibration control

Paolo Gardonio[a]
Cristóbal González Díaz[b]
Institute of Sound and Vibration Research
University of Southampton
Highfield, Southampton, SO17 1BJ (UK)

ABSTRACT

This paper presents a simulation study on the downscaling of multiple electro-dynamic proof mass actuators for the implementation of decentralised velocity feedback control loops on a thin panel. The system is conceived to reduce the panel response at low resonance frequencies. In the first part of the paper, the principal downscaling laws of a single proof mass actuator are revised. In particular, the scaling laws are given for: a) the fundamental natural frequency, b) the damping factor, c) the static displacement, d) the actuation force f_a and control force f_c, and e) the maximum stroke Δw_a. The second part of the paper presents a numerical study about the control performance produced by decentralised control systems with an increasing number of control units, which are scaled down in such a way as to keep the total base surface occupied by the actuators constant. This study shows that the control performance tends to rise as the number of control units is increased. However, this trend is reversed for large arrays of small scale actuators since the gain margin of the feedback loops tends to decrease with downscaling.

1. INTRODUCTION

Theoretical studies have shown that decentralised velocity feedback control with collocated and dual velocity sensor and force actuator pairs effectively reduce the response at low frequency resonances of the structure where they are mounted[1]. Therefore, this type of control system is particularly suited to control broad band random disturbances at low audio frequencies[2]. However, the practical implementation of multiple feedback loops using electro-dynamic proof mass actuators with accelerometer sensors at their footprints is limited by stability issues[3-5]. In particular Bauman and Elliott[4] have shown that the cross talking between neighbouring control units may lead to instability even if each control unit implements a control gain that ensures stability when the other units are turned off.

The aim of this paper is to investigate how the stability and control performance of a decentralised velocity feedback control system mounted on a plate varies with the downscaling of the electro-dynamic proof mass actuators. The downscaling study is carried out considering an increasingly denser array of smaller feedback control units so that the total area covered by the actuators remains constant as the size, and thus the base area, of the actuators is scaled down.

The paper is structured in three parts. Section 2 briefly describes the control system and the mathematical model used to perform the scaling study. Also, the stability and control performance of the *benchmark control configuration* with five decentralised control units

[a] Email address: pg@isvr.soton.ac.uk
[b] Email address: cgd@isvr.soton.ac.uk

considered in the study is revised. Section 3 introduces the principal downscaling laws for a single control actuator. Finally Section 4 presents the downscaling study considering an increasingly dense array of smaller control units.

2. MODEL PROBLEM

A. Control System

Figure 1a shows a schematic of the simply supported plate with *N* velocity feedback control units considered in this study. The geometrical and material properties of the plate and benchmark control system, which has five control units arranged along the diagonals and at the centre of the panel (Case (a) in Section 4), are given in Table 1. The plate is excited by a plane acoustic wave with incident and lateral angles of 45°. In this way, the natural modes of the plate are evenly excited. Each control unit is formed by a proof mass electro-dynamic actuator with an idealised velocity sensor located in correspondence to the centre of the actuator base. As shown in Figure 1b, the actuator is formed by a cylindrical mass suspended on elastic springs and a coil, which is fixed to a thin base disc. The mass is formed by a cylindrical core magnet and an outer ferromagnetic ring, which produce a radial magnetic field perpendicular to the coil winding. In order to maximize the magnetic field that couples with the coil winding, the inner and outer air gaps between the coil and the suspended mass are kept to a minimum that avoid friction.

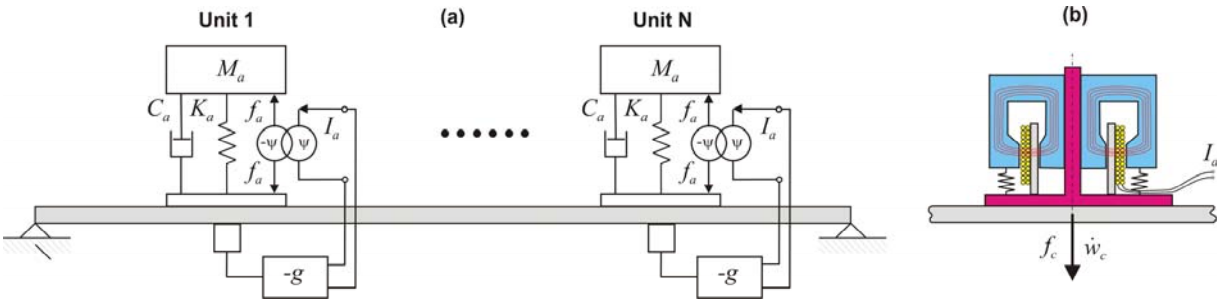

Figure 1: (a) Plate with N velocity feedback loops using proof mass actuator and velocity sensor pairs. (b) Schematic of the coil-magnet proof mass actuator.

Table 1: Geometry and physical parameters for the aluminium panel and benchmark control system.

Parameter	Value
Dimensions	$l_x \times l_y = 414 \times 314$ mm^2
Thickness	$h = 1$ mm
Mass density	$\rho = 2720$ kg/m^3
Young's modulus	$E = 7.1 \times 10^{10}$ N/m^2
Poisson ratio	$\nu = 0.33$
Damping loss factor	$\eta = 0.02$
Position control unit 1	$x_{c1} = 109$, $y_{c1} = 75$ mm
Position control unit 2	$x_{c2} = 109$, $y_{c2} = 239$ mm
Position control unit 3	$x_{c3} = 305$, $y_{c3} = 239$ mm
Position control unit 4	$x_{c4} = 305$, $y_{c4} = 75$ mm
Position control unit 5	$x_{c5} = 207$, $y_{c5} = 157$ mm

Table 2: Geometry and physical parameters for the reference control actuator.

Parameter	Value
Base disk diameter	$\phi_b = 38.4$ mm
Base disk height	$h_b = 1$ mm
Base disk mass	$M_b = 9.5$ g
Proof mass diameter	$\phi_a = 22.8$ mm
Proof mass height	$h_a = 11$ mm
Proof mass	$M_a = 24$ g
Springs Young modulus	$E_S = 9.2 \times 10^3$ N/m^2
Springs base area	$A_s = 84.8$ mm^2
Springs height	$h_s = 15$ mm
Springs stiffness	$K_a = 108.4$ N/m
Viscous damping coefficient	$C_a = 1.96$ N/ms^{-1}
Damping ratio	$\zeta_a = 0.6$
Voice coil factor	$\psi_a = 2.6$

The axial motion of the suspended mass is guided by a stinger. The dimensions and physical properties of the *reference actuator* for the benchmark control arrangement are given in Table 2. The actuator proof mass M_a has been calculated as that of a solid cylinder with the outer dimensions (diameter ϕ_a and height h_a) of the actual proof mass and an equivalent smeared density ρ_a. Also, the stiffness of the actuator suspension K_a has been derived as that of three elastomeric springs (with Young's modulus of elasticity E_s) in parallel with base area A_S and height h_S. The viscous damping coefficient C_a has been selected in such a way that the damping ratio ζ_a is 0.6. Finally the voice coil coefficient has been derived from the relation[6] $\psi_a = Bl_w$, assuming the actuator magnet produces a uniform magnetic flux density B across the windings of the coil with total length exposed to the magnetic flux l_w.

B. Mathematical Model

The steady state response of the panel with *N* control units due to a time harmonic primary acoustic wave excitation, with time dependence of the form $\mathrm{Re}\{\exp(j\omega t)\}$, where ω is the circular frequency and $j = \sqrt{-1}$, has been derived in terms of the time-averaged total flexural kinetic energy[2]:

$$T(\omega) = \frac{1}{4}\int_0^{l_x}\int_0^{l_y} \rho h \left|\dot{w}(x,y,\omega)\right|^2 dxdy \quad , \tag{1}$$

where ρ is the density of the material of the plate and l_x, l_y, h are respectively the dimensions and the thickness of the plate. The complex transverse velocity over the plate surface $\dot{w}(x,y,\omega)$, has been derived from a fully coupled model of the panel with the feedback control units using electro-mechanical impedance/mobility functions. The air fluid loading on the panel has been considered negligible. Assuming the system is linear, the velocity $\dot{w}(x,y,\omega)$ has been derived as the superposition of the response to the primary acoustic wave excitation and the response to the passive and active actions of the control units, which have been derived in terms of modal summations cast in the following matrix form:

$$\dot{w}(x,y,\omega) = \boldsymbol{\varphi}(x,y)\mathbf{A}_c(\omega)\mathbf{f}_c(\omega) + \boldsymbol{\varphi}(x,y)\mathbf{a}_p(\omega)p_i(\omega) \quad , \tag{2}$$

where $p_i(\omega)$ is the complex pressure of the incident acoustic wave, $\mathbf{f}_c(\omega) = \lfloor f_{c1}(\omega) \quad \cdots \quad f_{cN}(\omega) \rfloor^T$ is a column vector with the passive and active force effects exerted by the *N* control units, $\boldsymbol{\varphi}(x,y) = \lfloor \phi_1(x,y) \quad \cdots \quad \phi_R(x,y) \rfloor$ is a row vector with the first *R* modes of the panel at position (x,y) and finally $\mathbf{A}_c(\omega)$, $\mathbf{a}_p(\omega)$ are respectively a $[R \times N]$ matrix with the complex modal excitations functions generated by the forces exerted by the control units and a $[R \times 1]$ vector with the complex modal excitations functions generated by the incident plane wave. The elements in the matrix $\mathbf{A}_c(\omega)$ and vector $\mathbf{a}_p(\omega)$ are given by the following two expressions

$$A_{c_{r,n}}(\omega) = \frac{\phi_r(x_{cn}, y_{cn})}{M_p\left[\omega_r^2(1+j\eta) - \omega^2\right]} \quad , \qquad a_{p_r}(\omega) = \frac{2\int_0^{l_x}\int_0^{l_y} \phi_r(x,y) e^{-j(k_x x + k_y y)} dxdy}{M_p\left[\omega_r^2(1+j\eta) - \omega^2\right]} \quad . \tag{3,4}$$

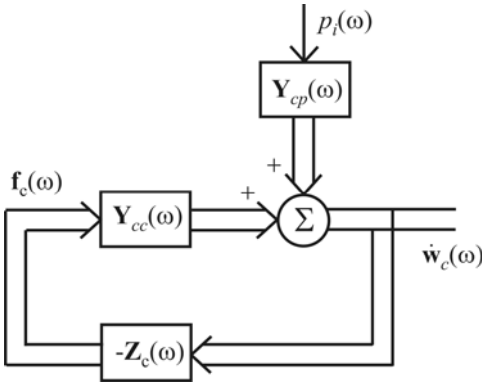

Figure 2: Block diagram of the multi-channel decentralised control system.

In these equations $M_p = \rho h l_x l_y$ is the mass of the plate, η is the loss factor, ω_r and $\phi_r(x_{cn}, y_{cn})$, $\phi_r(x, y)$ are respectively the *r*-th natural frequency and *r*-th mass-normalised natural modes of the plate at positions (x_{cn}, y_{cn}) and (x, y), which have been taken from reference[7] for a simply supported panel. Finally $k_x = k_o \sin(\theta)\cos(\phi)$ and $k_y = k_o \sin(\theta)\sin(\phi)$ are the wave numbers in x and y directions of the incident acoustic plane wave with azimuthal and elevation angles of $\phi = 45^o$ and $\theta = 45^o$, where $k_o = \omega / c_o$ and $c_o = 343\, m/s$ are respectively the acoustic wave number and speed of sound in air. The factor 2 in Eq. (4) accounts for the blocked pressure doubling of the incident acoustic wave[2]. The closed loop velocities and forces produced by the decentralised control units can be modelled in terms of the block diagram shown in Figure 2. Thus the column vector with the complex phasors of the velocities at the control positions $\dot{\mathbf{w}}_c(\omega) = \lfloor \dot{w}_{c1}(\omega) \quad \cdots \quad \dot{w}_{cN}(\omega) \rfloor^T$ is given by

$$\dot{\mathbf{w}}_c(\omega) = \mathbf{Y}_{cc}(\omega)\mathbf{f}_c(\omega) + \mathbf{Y}_{cp}(\omega)p_i(\omega) \ , \tag{5}$$

where $\mathbf{Y}_{cc}(\omega)$ is a fully populated matrix of point and transfer mobility functions between the control positions and $\mathbf{Y}_{cp}(\omega)$ is a column vector with the mobility functions between the control positions and the primary wave excitation. The elements of $\mathbf{Y}_{cc}(\omega)$ and $\mathbf{Y}_{cp}(\omega)$ are given by:

$$Y_{cc}^{i,j}(\omega) = j\omega \sum_{r=1}^{N} \frac{\phi_r(x_{ci}, y_{ci})\phi_r(x_{cj}, y_{cj})}{M_p\left[\omega_r^2(1+j\eta) - \omega^2\right]} \ , \quad Y_{cp}^{i}(\omega) = j\omega \sum_{r=1}^{N} \frac{\phi_r(x_{ci}, y_{ci}) 2 \int_0^{l_x}\int_0^{l_y} \phi_r(x, y) e^{-j(k_x x + k_y y)} dxdy}{M_p\left[\omega_r^2(1+j\eta) - \omega^2\right]} \ . \tag{6,7}$$

The vector with the passive and active forces exerted by the control units can be expressed as:

$$\mathbf{f}_c(\omega) = -\mathbf{Z}_c(\omega)\dot{\mathbf{w}}_c(\omega) \ , \tag{8}$$

where $\mathbf{Z}_c(\omega)$ is a diagonal matrix with the point impedances of the closed loop control units. Assuming the control actuators are current driven, these point impedances are given by[8]

$$Z_c(\omega) = \frac{1}{Y_b(\omega)} + \frac{Z_a(\omega) + \psi_a g}{1 + Y_a(\omega)Z_a(\omega)} \ , \tag{9}$$

where $Z_a(\omega) = C_a + K_a / j\omega$ $Y_a(\omega) = 1/ j\omega M_a$ and $Y_b(\omega) = 1/ j\omega M_b$ are respectively the impedance of the suspension springs and the mobilities of the proof mass and base mass and g is the frequency independent control gain. Finally K_a and C_a are the stiffness and damping coefficient of the elastic springs and M_a and M_b are the proof mass and base mass respectively. After some mathematical manipulations the vectors with the control velocities and control forces are found to be given by

$$\dot{\mathbf{w}}_c(\omega) = \left(\mathbf{I} + \mathbf{Y}_{cc}(\omega)\mathbf{Z}_c(\omega)\right)^{-1}\mathbf{Y}_{cp}(\omega)p_i(\omega) \ , \ \mathbf{f}_c(\omega) = -\mathbf{Z}_c(\omega)\left(\mathbf{I} + \mathbf{Y}_{cc}(\omega)\mathbf{Z}_c(\omega)\right)^{-1}\mathbf{Y}_{cp}(\omega)p_i(\omega). \tag{10,11}$$

Thus after substitution of Eq. (11) into Eq. (2) and then the resulting Equation into Eq. (1), the total kinetic energy of the panel with the decentralised control units is derived as

$$T(\omega) = \frac{M_p}{4}\left|p_i(\omega)\right|^2\left[\mathbf{A}_c(\omega)\mathbf{Q}_c(\omega) + \mathbf{a}_p(\omega)\right]^H\left[\mathbf{A}_c(\omega)\mathbf{Q}_c(\omega) + \mathbf{a}_p(\omega)\right] \ , \tag{12}$$

where $\mathbf{Q}_c(\omega) = -\mathbf{Z}_c(\omega)\left(\mathbf{I} + \mathbf{Y}_{cc}(\omega)\mathbf{Z}_c(\omega)\right)^{-1}\mathbf{Y}_{cp}(\omega)$ and the integrals of the natural modes over the surface area of the panel have resulted in the mass of the plate constant M_p since the natural modes are mass normalized so that $\rho h\int_0^{l_x}\int_0^{l_y}\phi_i\phi_j dxdy = 0$ and $\rho h\int_0^{l_x}\int_0^{l_y}\phi_i\phi_i dxdy = \rho h l_x l_y = M_p$.

C. Stability Analysis

The practical implementation of a velocity feedback control loop with a proof mass electro-dynamic actuator is characterised by a low frequency stability problem[3,4,9]. This is due to the fact that in order to produce a constant actuation force in phase with the driving signal, the actuator is designed with a low fundamental natural frequency below the first resonance of the structure under control. At low frequencies up to the fundamental resonance of the actuator, the control force produced by the actuator is out of phase with the driving signal. In other words the actuator control force is not dual to the error velocity measured at the base of the actuator[10,11]. Thus, if a negative velocity feedback loop is implemented, a positive velocity feedback is produced at low frequencies, which may lead to instability for high control gains. The maximum gain that would ensure stability can be derived from the Bode or Nyquist plots of the open loop sensor–actuator frequency response function (FRF), which are shown in Figure 3 for the control loop N. 1 of the

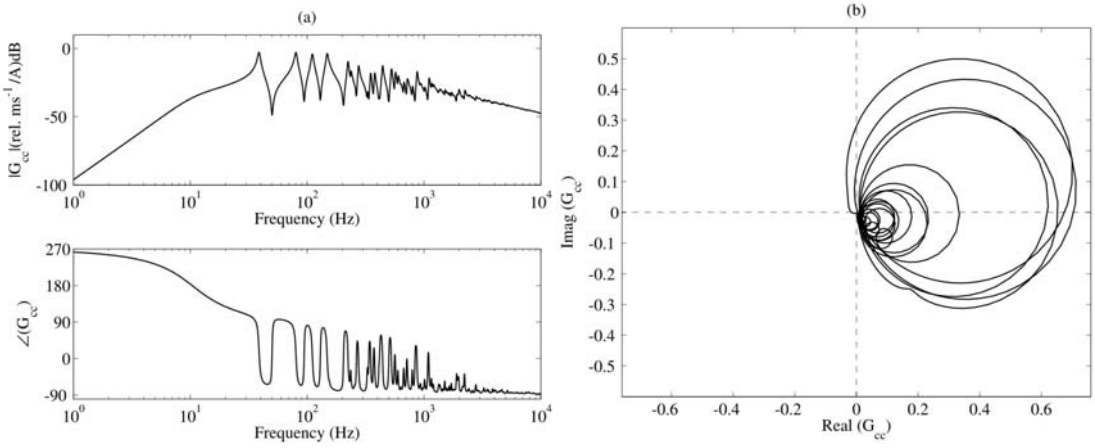

Figure 3: Bode (a) and Nyquist (b) plots of the open loop sensor–actuator FRF of the control loop N 1.

benchmark control configuration. The two plots highlight that, at frequencies below the first resonance of the panel, at 39 Hz, the FRF is real negative and would encircle the Nyquist stability point (-1, *j*0) when the gain is $g_{\max 1} = 64.6$. The Bode plot of the FRF shows that the fundamental resonance of the actuator, around 10 Hz, is highly damped. This is a desirable effect since it tends to reduce the amplitude of the real negative portion of the FRF and thus, as can be noted in the Nyquist plot, larger feedback control gains can be implemented.

Balas[12] has shown that multiple decentralised velocity feedback control loops would be unconditionally stable if the sensor–actuator pairs are dual and collocated[10,11]. As discussed above, the control force produced by the proof mass electro-dynamic actuator is not dual to the error velocity and thus stability of multiple feedback loops is not guaranteed. Baumann and Elliott[4] have also shown that when multiple feedback loops are implemented simultaneously, the maximum feedback control gains that ensure stability are lower than those that ensure stability of each control unit in isolation.

The stability of multiple channel feedback control loops is normally assessed with the generalised Nyquist stability criterion[13], which states that, assuming both the plant and controller are individually stable, a multichannel feedback system is bound to be stable provided the locus of $\det(\mathbf{I} + \mathbf{Y}_{cc}\mathbf{Z}_c)$ does not encircle the instability point (0, *j*0) as ω varies from $-\infty$ to $+\infty$. Figure 4a shows that the locus of $\det(\mathbf{I} + \mathbf{Y}_{cc}\mathbf{Z}_c)$ for the system with five control units may encircle the instability point (0, *j*0) for large control gains. The maximum gain that would ensure stability has been derived by plotting the eigenvalues $\lambda_1, \ldots, \lambda_5$ of $\mathbf{Y}_{cc}\mathbf{Z}_c$ assuming $g = 1$. In fact $\det(\mathbf{I} + \mathbf{Y}_{cc}\mathbf{Z}_c) = (1 + g\lambda_1)\cdots(1 + g\lambda_5)$ and thus the maximum feedback control gain can be derived from the locus of the largest eigenvalue of $\mathbf{Y}_{cc}\mathbf{Z}_c$. In this case stability is ensured if the locus does not encircle the instability point (-1, *j*0). The plot with the five eigenvalues shown in Figure 4b indicates that the maximum control gain of the five channels feedback system is $g_{\max 5} = 17.1$; thus about 3.8 times smaller than that ensuring stability of one control unit.

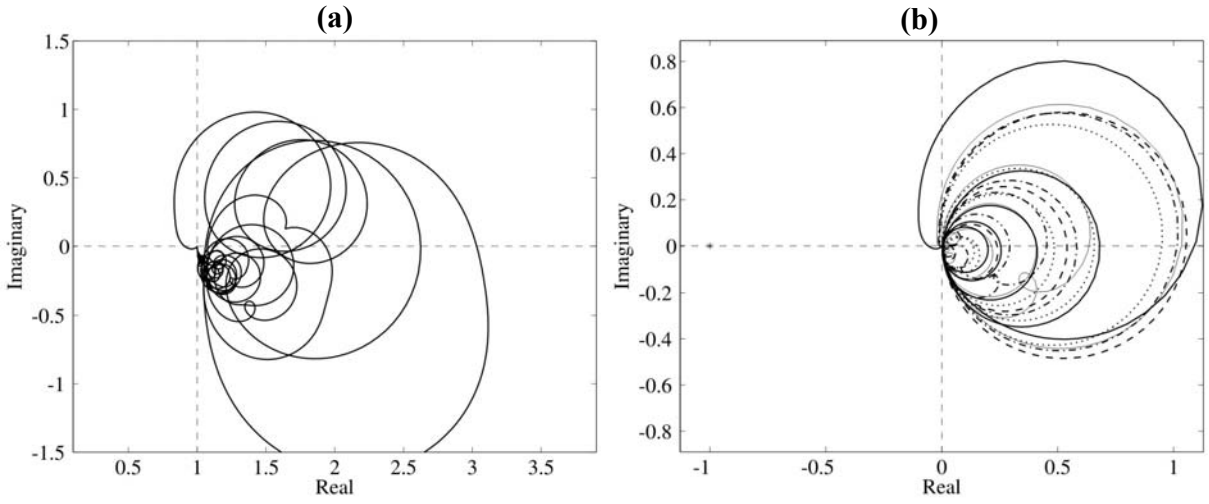

Figure 4: (a) Locus of *det*(**I**+$\mathbf{Y}_{cc}\mathbf{Z}_c$). (b) Loci of the five eigenvalues of $\mathbf{Y}_{cc}\mathbf{Z}_c$

D. Control Performance

The plot in Figure 5 shows the spectrum of the flexural kinetic energy per unit acoustic incident wave in a frequency range between 1 Hz and 1 kHz. The dashed line shows that, when the five control gains are gradually increased from zero the response of the panel tends to go down at low resonance frequencies as a result of the active damping action produced by the velocity feedback loops, which efficiently absorbs energy from the panel at these frequencies. The dotted line shows the response of the panel when the maximum stable control gain is implemented in the five control loops. In this case, around the fundamental resonance frequency of the proof mass actuators, the positive velocity feedback effect produced by the actuator dynamics effectively enhances the response so that a rather high and sharp peak is produced at 10 Hz. If a higher control gain was implemented, the system would go unstable and produce large vibrations at the fundamental resonance of the actuator. The faint line shows the best control performance averaged in the 1 Hz to 1 kHz frequency band, which for the benchmark control system with five actuators is produced by a control gain close to the maximum gain that ensures stability. Large kinetic energy reductions up to 30 dB are obtained for the first two resonances. Also, smaller reductions between 5 and 10 dB are produced at higher resonances in the frequency range under consideration. However, the positive feedback effect at the fundamental resonance frequency of the actuators has enhanced the response by about 10 dB around 10 Hz.

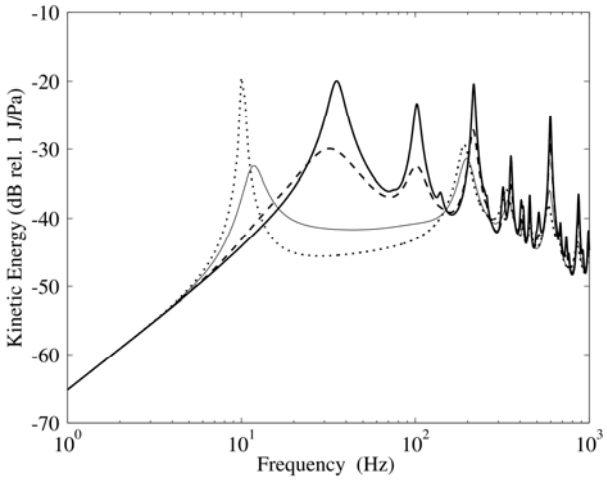

Figure 5: Panel Kinetic Energy per unit sound pressure of the incident acoustic wave. No control (thick line), small feedback gains (dashed line), optimal control gain (faint line) very large control gain (dotted line).

3. DOWNSCALING OF ONE CONTROL UNIT

The downscaling laws for the main components and for the principal physical properties of the actuator have been derived in references[14-17] and are summarised in Tables 3 and 4 using the $[L^n]$ notation described by Madou[15], where n identifies the power of the linear dimension L. For those quantities that remain unchanged with scaling, a $[L^0]$ scaling law is assigned. The scaling of the current density in the coil windings is taken from Trimmer[16] for the case of constant temperature difference, ΔT, between the windings of the coil and the surrounding environment. Also, the scaling of the damping coefficient is taken from Peirs[17] assuming squeeze film damping below the cut-off frequency ω_c (below ω_c, damping force is higher than elastic force in squeezed films). The downscaling of the control force is derived at frequencies above

the fundamental resonance frequency of the proof mass actuator where the feedback loop is designed to operate. Assuming a blocked base and $\zeta_a < 1$, above the resonance frequency of the actuator the actuator control force is given by[14]:

$$f_c(\omega > \omega_a) \approx f_a = \psi_a i_a \quad , \tag{13}$$

The downscaling of the actuator stroke is derived for the maximum stroke that occurs at the fundamental resonance frequency of the proof mass actuator. Also in this case, assuming a blocked base, the stroke of the actuator at the fundamental resonance frequency of the actuator is given by[14]:

$$\Delta w_a(\omega_a) \approx \psi_a i_a / \omega_a^2 M_a \zeta_a \quad , \tag{14}$$

The plots in Figure 6 show the downscaling laws of the electro-mechanical properties that directly influence the stability and control performance of a feedback loop with a proof mass electro-dynamic actuator. The downscaling laws are plotted with respect to the downscaling of the actuator base disc diameter, which is normalized to that of the reference actuator whose dimensions and physical properties are listed in Table 2.

Table 3: Downscaling laws of the main components of the proof mass electro-dynamic actuator.

Parameter	Expression	Downscaling
Proof mass	$M_a = \rho_m \pi \phi_m^2 h_m / 4$	$M_a \propto [L^3]$
Suspension stiffness	$K_a = 3E_s A_s / h_s$	$K_a \propto [L^1]$
Damping coefficient	From ref.[17]	$C_a \propto [L^1]$
Current density in the coil	From ref.[16]	$J_a \propto [L^{-1}]$
Current in the coil	$i_a = J_a A_w$	$i_a \propto [L^1]$
Voice coil coefficient	$\psi_a = Bl_w$	$\psi_a \propto [L^1]$

Table 4: Downscaling laws of the principal physical properties of the proof mass electro-dynamic actuator.

Parameter	Expression	Downscaling
Fundamental natural frequency	$\omega_a = \sqrt{K_a / M_a}$	$\omega_a \propto [L^{-1}]$
Damping ratio	$\zeta_a = C_a / 2\sqrt{K_a M_a}$	$\zeta_a \propto [L^{-1}]$
Static displacement	$\delta_a = M_a g / K_a$	$\delta_a \propto [L^2]$
Actuation force	$f_a = -\psi_a i_a$	$f_a \propto [L^2]$
Maximum stroke	$\Delta w(\omega_a) \approx \psi_a i_a / \omega_a^2 M_a \zeta_a$ *	$\Delta w_a \propto [L^2]$
Control force	$f_c(\omega > \omega_a) \approx \psi_a i_a$ *	$f_c \propto [L^2]$

* mobility of base structure assumed equal to zero, i.e. blocked base

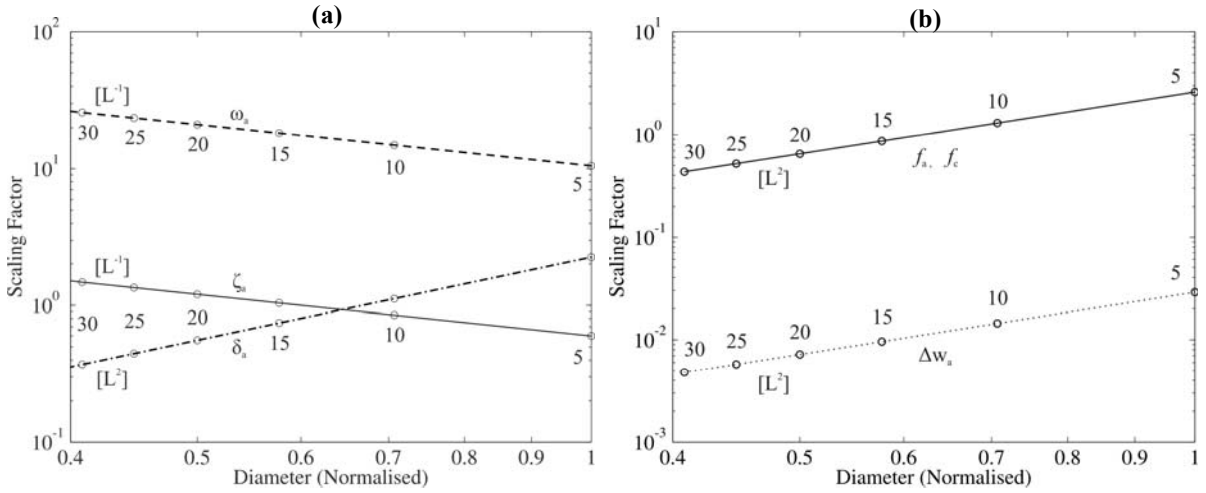

Figure 6: Downscaling laws of (plot a) actuator fundamental natural frequency ω_a, (dashed line) static displacement δ_a (dash-dotted line), damping ratio ζ_a (faint line) and (plot b) actuation and control forces f_a and f_c (faint line) maximum stroke Δw_a (dotted line).

The graphical representation of these downscaling laws suggests the following observations.

1) The fundamental natural frequency of the actuator ω_a rises linearly with the downscaling of the actuator. Therefore the actuator can be downscaled only to a size where the fundamental natural frequency approaches the first resonance frequency of the structure under control.
2) The damping ratio ζ_a also rises linearly as the size of the actuator is scaled down. This is a desirable effect since it tends to smooth the peak of the actuator fundamental resonance, which, as shown in the two plots of Figure 3, determines the gain margin of the feedback loop.
3) The static displacement of the suspended mass δ_a decreases quadratically with the downscaling of the actuator. This is also a desirable effect since it reduces the sag of the suspended mass produced by quasi static displacements of the structure under control.
4) For $\omega > \omega_a$ the actuation and control forces, f_a and f_c, decrease quadratically as the size of the actuator is scaled down. According to Eq. (13) and the scaling laws in Table 3, this is due to the combination of two effects: first, the maximum current that can be fed to the actuator i_a decreases linearly with the downscaling and, second, the electro-mechanical actuation coefficient ψ_a also decreases linearly with the downscaling.
5) The maximum stroke $\Delta w_a(\omega_a)$ also decreases quadratically with the downscaling of the actuator. Thus the dynamic stroke falls at a higher rate than that of the clearance allowed for the axial vibration of the suspended mass, which falls down linearly with the downscaling of the actuator. Although from the constructive point of view this is a desirable effect, as discussed in point 4) above, in practice it is associated with the reduction of the actuation and thus control force that can be generated by the actuator.

In order to avoid the instability problem generated by the low frequency resonance of the actuator, an alternative suspension system should be used. For example, a non linear suspension system could be used, with small stiffness for the dynamic vibration range of the proof mass and a finite stiffness effect outside this range that provides end stops for unpredicted large oscillations of the proof mass and during pause condition of the feedback loop. However,

Bauman and Elliott[18] have shown that if the suspended mass was to hit the stiff end stops during operation, the feedback loop may become unstable.

In order to improve the control performance of the feedback loop, the use of an alternative actuation transducer that scales linearly with the downscaling of the actuator size would also be preferable. In practice linear downscaling of actuation forces is possible with micro-scale electrostatic actuators[15-17]. For instance the force produced by a parallel plate electrostatic actuator decreases linearly with the downscaling of the actuator provided the gap between the plates is of the order of 100 μm, in which case the breakdown voltage is rather small and may be considered constant. Thus this type of actuator would produce small forces and work only with a micro-scale proof mass actuator whose natural frequency is bound to be much higher than the fundamental resonance frequency of the structure under control.

3. DOWNSCALING OF MULTIPLE CONTROL UNITS

The downscaling study of multiple control units has been carried out assuming an increasingly denser array of smaller control units so that the total area covered by the actuators base disc remains the same. As shown in Figure 7, six configurations with 5, 10, 15, 20, 25 and 30 control units have been considered (locations and size of the control units are drawn to scale). The principal dimensions and physical properties of the proof mass actuators used in these six configurations are summarised in Table 5. The plots in Figure 8 contrast the downscaling laws for the base area and mass of a single actuator and for the whole set of actuators. This plot highlights that, when the downscaling of the actuators is accompanied by an increasing number of control units such that as the actuators are downscaled, a) the total the area covered by the actuators disc remains constant, b) the total mass of the control units decreases linearly and c) the total control force remains constant. Thus, despite the total area covered by the multiple actuators remaining the same, the total seismic mass available to produce the control force goes down linearly rather than cubically as it would for a fixed number of control units. Also the total control force remains constant instead of falling down quadratically as it would for a fixed number of control units.

Table 5: Principal geometrical and physical properties of the actuators used in the six control configurations.

Parameter	5 Act.	10 Act.	15 Act.	20 Act.	25 Act.	30 Act.
ϕ_a (proof mass) [mm]	22.8	16.1	13.2	11.4	10.2	9.3
h_a [mm]	11	7.8	6.3	5.5	4.9	4.5
M_a[g]	24.7	8.8	4.7	3.1	2.2	1.7
ϕ_b (base) [mm]	38.4	27.1	22.2	19.2	17.2	15.7
h_b[mm]	1	0.7	0.6	0.5	0.45	0.4
M_b[g]	*9.5*	*3.4*	*1.8*	*1.2*	*0.8*	*0.6*
K_a [N/m]	108.4	76.6	62.6	54.2	48.5	44.2
C_a [N/ms^{-1}]	1.9	1.4	1.1	0.98	0.9	0.8
ζ_a	0.6	0.8	1.0	1.2	1.3	1.5
f_a [Hz]	10.5	14.9	18.3	21.1	23.6	25.8
ψ_a [N/A]	2.6	1.8	1.5	1.3	1.2	1.1

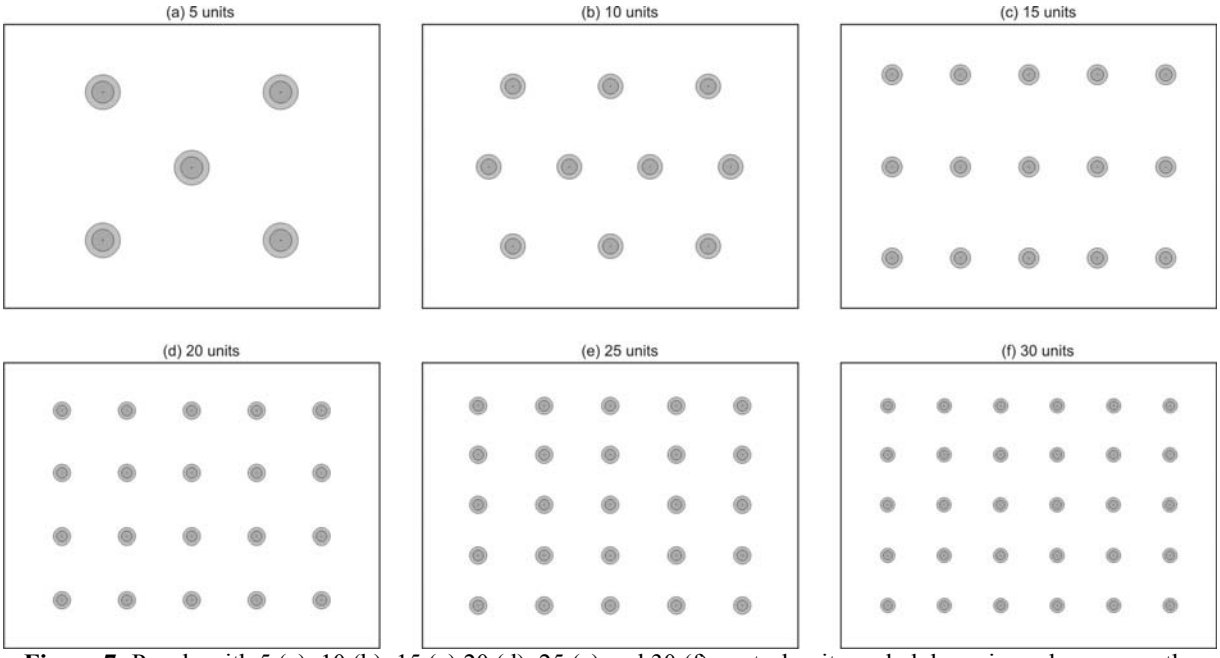

Figure 7: Panels with 5 (a), 10 (b), 15 (c) 20 (d), 25 (e) and 30 (f) control units scaled down in such a way as the total base area is keep constant. Positions of control units are drawn to scale.

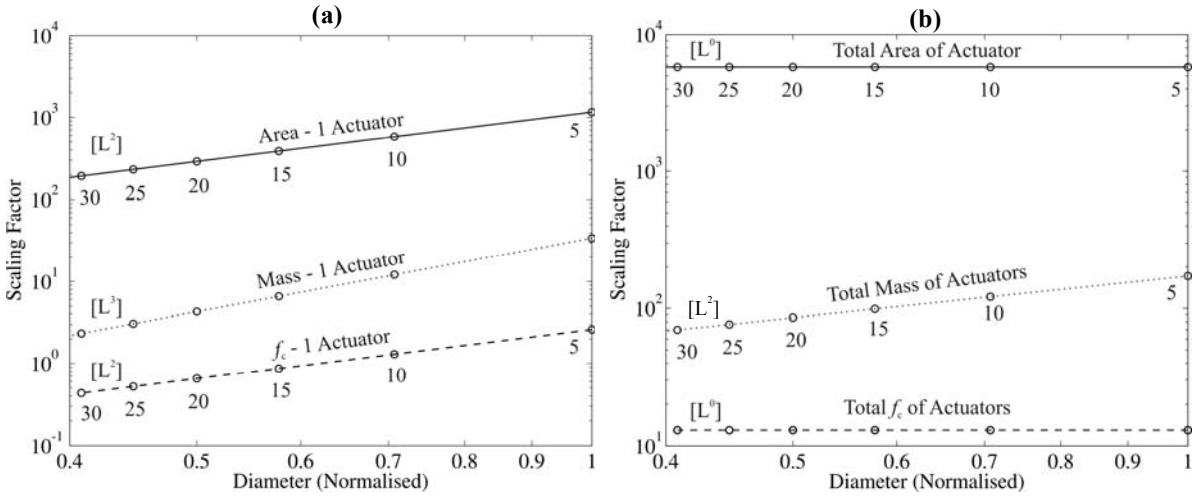

Figure 8: Downscaling laws of base area (solid lines), mass (dotted line) and control force (dashed line) of one actuator (plot a) and *N* actuators (plot b).

The performance of the multiple feedback control loops with increasingly smaller control units has been assessed by plotting the normalised[‡] total kinetic energy integrated from 1 Hz to 1 kHz as a function of the feedback control gain g in the feedback loops. As shown in Figure 9, the plots have been derived for a wide range of control gains between 10^{-2} and 10^{4} regardless of the stability condition. All plots show that as the control gains are raised from zero, the kinetic energy of the panel tends to decrease up to an optimal control gain g_{opt} (marked by a square) above which it tends to go up again. This phenomenon has been investigated in previous works[1,3]

[‡] Normalised to the total kinetic energy when the feedback control loops are left open

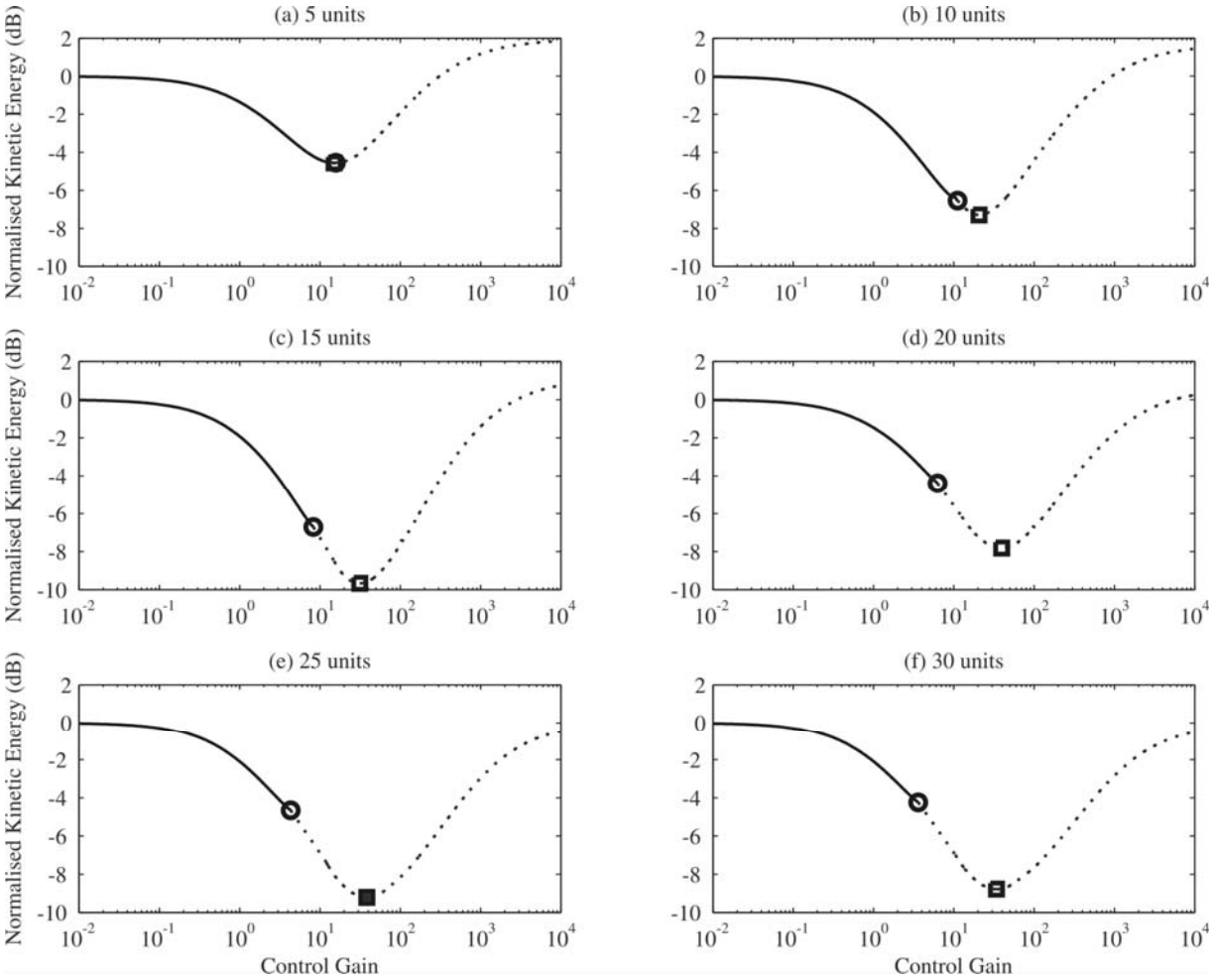

Figure 9: Normalised Kinetic Energy averaged between 10 Hz and 1 kHz for the systems with 5, 10, 15 20, 25, 30 control units. Circle markers: maximum stable gain; square markers: optimal control gain. Solid line: stable gains; dotted lines: unstable gains.

which have shown that, when the optimal feedback control gain is exceeded, the active damping produced by the control units tends to diminish since the vibration at the control position is brought down by the controller. As a result, the response of the panel again tends to become lightly damped with sharp resonance frequencies, which occur at higher frequencies since the simply supported panel is now constrained at the control positions[19]. However, in practice, the control units can hardly implement the optimal control gains that would give the best control performance[5]. The stability limit for each configuration of the control units has been derived with reference to the generalized Nyquist stability criterion by plotting the locus of the largest eigenvalue of $\mathbf{Y}_{cc}\mathbf{Z}_{c}$ as described in Section 2.C. The maximum stable control gains $g_{\max}$ for each control configuration has been marked with a circle and the part of the curve for the fictitious reduction of Kinetic Energy that would be produced by unstable feedback loops has been represented with a dotted line. The six plots in Figure 9 show that, apart from the first configuration with five control units, the optimal and maximum stable control gains clearly diverge from each other. As a result also the optimal and maximum reductions of kinetic energy move away from each other.

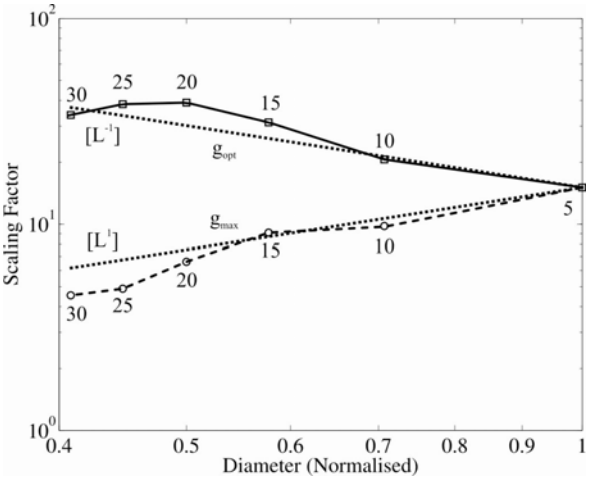

Figure 10: Maximum stable gains (dashed line) and optimal control gains (solid line) produced by actuators downscaling. Dotted lines obtained with line fitting.

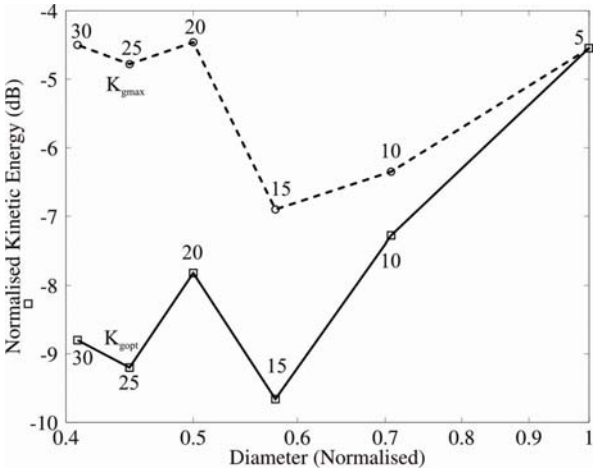

Figure 11: Reduction of kinetic energy for maximum stable gains (dashed line) and optimal control gains (solid line) produced by actuators downscaling.

These trends are exemplified in Figures 10 and 11. As the size of the control units is reduced and the number of control units is increased the optimal control gain tends to go up linearly. As a result, the optimal control performance tends to augment as the number of downscaled control units is increased although only up to the system with 15 units, which produces about double reduction of kinetic energy compared with that of the system with 5 control units (from 4.6 dB to 9.6 dB). Systems with more than 15 control units show smaller reductions which do not fit into a smooth curve since the passive response of the panel can change significantly from one control configuration and another.

Nevertheless the plot in Figure 10 indicates that in practice the maximum control gain that ensures stability of the feedback control loops goes down linearly. As a result, the plot in Figure 11 indicates that the actual reduction of kinetic energy that can be generated by the maximum control gain is lower than that produced with the optima control gain. The best performance is still achieved by the system with 15 control units, which produces about 7 dB reduction.

4. CONCLUSIONS

This paper has presented a simulation study about the implementation of decentralised velocity feedback control with an increasing number of control units using smaller scale proof mass electro-dynamic actuators. The actuators have been progressively scaled down in such a way that the total area covered by the actuators remains constant. It has been shown that the down scaling of a proof mass electro-dynamic actuator produces positive (increment of internal damping and reduction of both static displacement and stroke) and negative (increment of the fundamental resonance frequency and reduction of actuation and control forces) effects for the implementation of velocity feedback control. The damping, static displacement and fundamental resonance frequency characteristics depend on the physical properties of the proof mass actuation system. The stroke, actuation force and control force depend on the physical properties of the actuation transducer reacting between the base disc and proof mass. As a result of these positive and negative effects, the implementation of increasingly denser arrays of smaller scale control units tends to produce higher control performance up to a system with 15 control units, which produces about 7 dB reduction compared to the 4.4 dB reduction of the reference system

with 5 control units. This is an interesting result, particularly in view of the fact that the control system with 15 actuators is 1.75 times lighter than that with 5 actuators.

ACKNOWLEDGEMENTS

This work was supported by the Platform Grant project "Structural Acoustics" funded by the Engineering and Physical Sciences Research Council (EPSRC) in the UK.

REFERENCES

[1] S. J. Elliott, P. Gardonio, T. C. Sors, and M. J. Brennan, "Active vibroacoustic control with multiple local feedback loops," *J. Acoust. Soc. Am.* **111** (2), 908-915 (2002).

[2] F. J. Fahy and P. Gardonio, *Sound and structural vibration: radiation, transmission and response.* (Academic Press, London, 2nd ed. 2007).

[3] C. Gonzalez Diaz and P. Gardonio, "Feedback control laws for proof-mass electro-dynamic actuators," *Journal of Smart Materials and Structures* **16**, 1766-1783 (2007).

[4] O. Baumann and S. J. Elliott, "The stability of decentralized multichannel velocity feedback controllers using inertial actuators," *Journal of the Acoustical Society of America* **121** (1), 188-196 (2007).

[5] C. Gonzalez Diaz, C. Paulitsch and P. Gardonio, "*Smart panel with active damping units. Implementation of decentralized control,*" *J. Acoust. Soc. Am.* **124**(2), 898-910 (2008).

[6] A. Preumont, *Mechatronics Dynamics of Electromechanical and Piezoelectric Systems.* 1 ed. Dordrecht, The Netherlands: Springer (2006).

[7] P. Gardonio and M. J. Brennan, "Mobility and impedance methods in structural dynamics," in F. J. Fahy and J. Walker *Advanced applications in acoustics, noise and vibration* London: E & FN Spon, 2004, 387-388, Chapter 9.

[8] J. Rohlfing and P. Gardonio, "Comparison of homogeneous and Sandwich panels with decentralised velocity feedback control units," *Noise and Vibration: Emerging Methods NOVEM 2009*, Keble College, Oxford, 5–8 April 2009.

[9] S.J. Elliott, M. Serrand and P. Gardonio, "Feedback stability limits for active isolation systems with reactive and inertial actuators", *ASME Journal of Vibration and Acoustics.* **123**, 250-261 (2001).

[10] J. Q. Sun, "Some observations on physical duality and collocation of structural control sensors and actuators," *Journal of Sound and Vibration*, **194**, 765-770 (1996)

[11] V. Jayachandran and J. Q. Sun, "Unconditional stability domains of structural control systems using dual actuator-sensor pairs," *Journal of Sound and Vibration* **208**(1), 159-166 (1997)

[12] M. J. Balas, "Direct velocity control of large space structures," *Journal of Guidance and Control* **2**, 252-253 (1979)

[13] S. J. Elliott. *Signal Processing for Active Control.* 1 ed. London: Academic Press (2001).

[14] C. Gonzalez Diaz, C. Paulitsch and P. Gardonio, *"Active damping control unit using a small scale proof mass electrodynamic actuator," J. Acoust. Soc. Am.* **124**(2), 886-897 (2008).

[15] M. J. Madou. *Fundamentals of microfabrication: the science of miniaturization.* 1st ed.CRC Press, Boca Raton (1997).

[16] W. S. N. Trimmer, "Microrobots and micromechanical systems," *Sensors and Actuators* **19** (3): 267-287 (1989).

[17] J. Peirs, "Design of micromechatronic systems: scale laws, technologies, and medical applications" (PhD Thesis, Katholieke Universiteit Leuven, 2001).

[18] O. Baumann and S. J. Elliott, "Destabilization of velocity feedback controllers with stroke limited inertial actuators," *Journal of the Acoustical Society of America* **121** (5), 211-217 (2007).

[19] P. Gardonio and S. J. Elliott, "Modal response of a beam with a sensor-actuator pair for the implementation of velocity feedback control," *Journal of Sound and Vibration* **284**(1-2) 1-22 (2005).